OPEN ACCESS

Salt Diffusivity in a Cu-Cellulose Nanofiber Based, Multi-Component Electrolyte Assessed Using Restricted Diffusion, Molecular Dynamics, and Nuclear Magnetic Resonance

To cite this article: Keith Duncan *et al* 2026 *J. Electrochem. Soc.* **173** 040501

View the article online for updates and enhancements.

You may also like

- Structural and Dynamical Insights of Cu-Coordinated Cellulose Nanofibers for Li^+ Battery by NMR Spectroscopy
Mounesha N Garaga, Lin Xu, Liangbing Hu et al.
- Synthesis of Cellulose Nanofibers for Solid Electrolytes: Advancing Sustainable Energy Storage
Julian Ignacio Lopez
- Cu^{2+}-Crossliked Cellulose Nanofiber Electrolyte for Sustainable Solid-State Supercapacitors
Ridwan T Ayinla, Islam Elsayed and El barbary Hassan

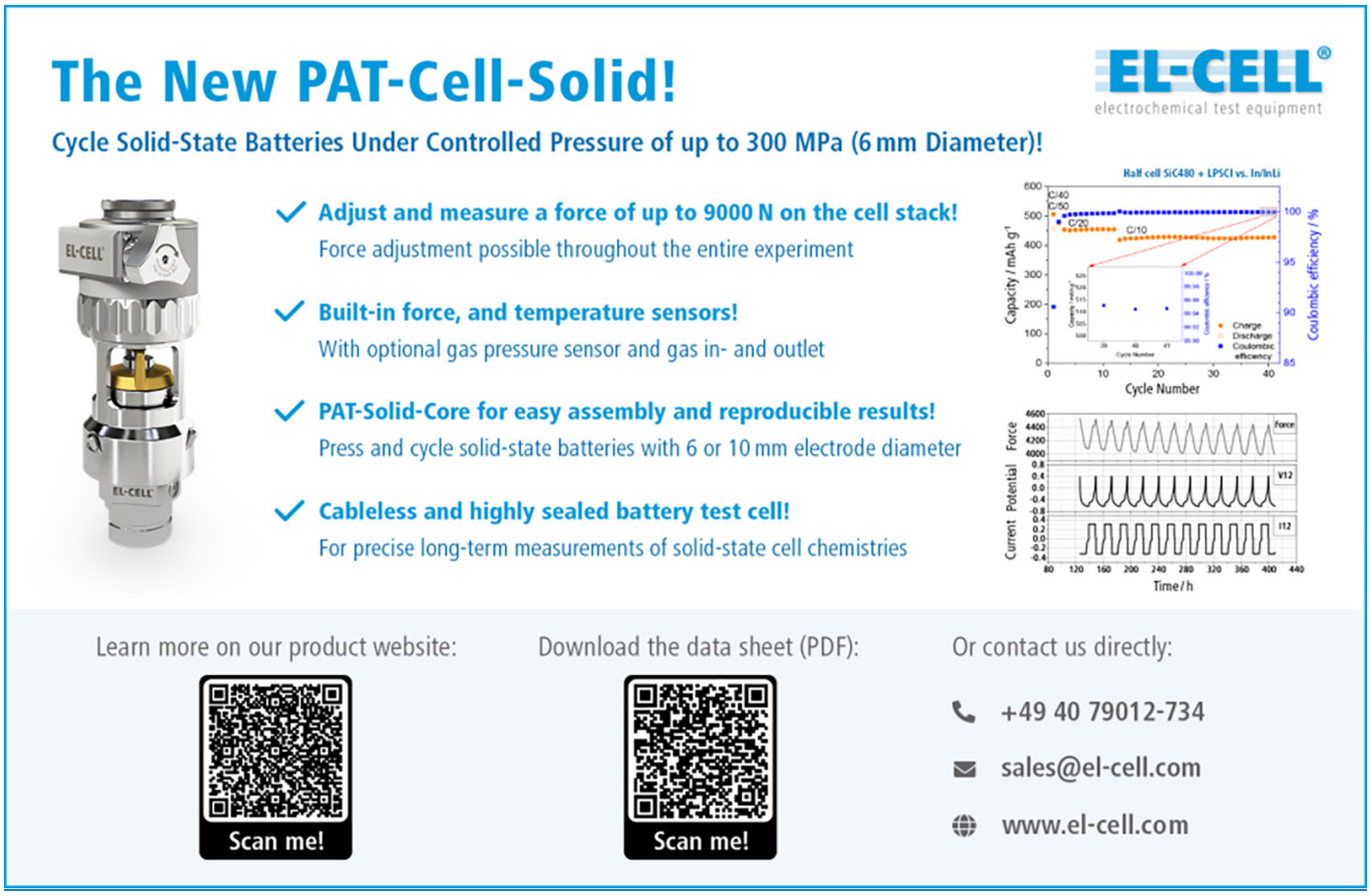

Journal of The Electrochemical Society, 2026 **173** 040501

Salt Diffusivity in a Cu-Cellulose Nanofiber Based, Multi-Component Electrolyte Assessed Using Restricted Diffusion, Molecular Dynamics, and Nuclear Magnetic Resonance

Keith Duncan,[1] Qisheng Wu,[2] Mounesha Garaga,[3] Michael McKee,[1] Lin Xu,[4,5,6] Xueying Zheng,[7] Aysha Siddika Asha,[2] Yue Qi,[2] Steven Greenbaum,[3] Liangbing Hu,[4,5,6] and Paul Albertus[1,z]

[1]*Department of Chemical and Biomolecular Engineering, University of Maryland, College Park, Maryland, United States of America*
[2]*School of Engineering, Brown University, Providence, Rhode Island 02912, United States of America*
[3]*Department of Physics, Hunter College: New York, New York, United States of America*
[4]*Department of Electrical and Computer Engineering, Yale University, New Haven, Connecticut 06511, United States of America*
[5]*Department of Materials Science, Yale University, New Haven, Connecticut, 06511, United States of America*
[6]*Center for Materials Innovation, Yale University, New Haven, Connecticut 06511, United States of America*
[7]*Department of Materials Science and Engineering, University of Maryland, College Park, Maryland 20742, United States of America*

Cu^{2+}-doped cellulose nano fiber (Cu-CNF) solid electrolytes were developed for fast charge, high energy density batteries. Cellulose chains in the fibers are opened by Cu^{2+} coordination, and a binary salt (LiTFSI) was added with minimal residual solvent left after the drying process. The Li^+ and $TFSI^-$ transport both within and between fibers greatly enhances the ion transport. To advance understanding of salt transport in Cu-CNF electrolytes, we conducted restricted diffusion experiments on two formulations of Cu-CNF samples to obtain the binary salt diffusivity ($D_\pm$) vs temperature, and measured the influences of test protocols and sample-to-sample variation. In addition, we did pulsed field gradient (PFG) nuclear magnetic resonance (NMR) experiments and used molecular dynamics (MD) simulations to model species motion. Restricted diffusion experiments show the Cu-CNF materials display concentration polarization voltage relaxation, and the resulting salt diffusivity is $D_\pm \approx 5 \times 10^{-12}$ m^2 s^{-1} at 45 °C, with $E_a \approx 0.55$ eV. PFG-NMR resulted in values for D_{Li+} and D_{TFSI-} with a similar magnitude to $D_\pm$, while MD (focused on intra-fiber transport) gave lower ion diffusivities and activation energies. The multi-component, fiber-based structure of these electrolytes provides new opportunities for transport theory and measurements, with future work focused on studying composition-property relationships to better quantify transport mechanisms.

 [DOI: 10.1149/1945-7111/ae4275]

Manuscript submitted September 15, 2025; revised manuscript received January 16, 2026. Published February 16, 2026.

Supplementary material for this article is available online

List of Symbols

Symbols

$D_\pm$	Salt diffusivity
G	gradient strength
I	Intensity with the field gradient
I_0	Intensity without field gradient
L	Electrolyte thickness
T	Time
V	Cell voltage
V_{offset}	Offset voltage
Γ	gyromagnetic ratio
Δ	gradient duration
Δ	diffusion time

Abbreviations

AGU	Anhydroglucose Unit
Cu-CNF	Copper doped cellulose nanofibers
DFT	Density function theory
DMC	Di-methyl carbonate
E-1	The first of two Cu-CNF formulations
E-2	The second of two Cu-CNF formulations
EC	Ethylene Carbonate
FEC	Fluorinated ethylene carbonate
LiTFSI	Lithium bis(trifluoromethanesulfonyl)imide
MD	Molecular dynamics
NMR	Nuclear magnetic resonance
NPT	Number, pressure, and temperature
NVT	Number, volume, and temperature
PFG	Pulse field gradient
RD	Restricted Diffusion
SEI	solid electrolyte interphase
SSE	Solid state electrolyte

Rechargeable batteries are in the process of revolutionizing both transportation and the grid-electricity sectors. Demand for Li-ion batteries in 2030 is projected to range from about 3–9 TWh yr^{-1} worldwide.[1–3] State of the art Li-ion battery packs can be recharged for >1000 cycles with high charge/discharge rates and high energy content.[2,4,5] Nevertheless, for greater adoption and utility, especially in the transportation sector, it is desired to increase both the specific energy (to >400 Wh kg^{-1}) and the charging rates (to >4 C). Greater specific energy increases the range of EVs and higher charging rates reduce the wait time for recharging. Consequently, there is concerted effort in battery research to develop superior anodes, cathodes and electrolytes to accomplish these goals.

There is significant electrolyte research work underway that is focused on inorganic glass and crystalline solid-state electrolytes (SSEs). (Note: see below for a table of abbreviations) SSEs generally have high transference numbers, in many cases equal to unity. Higher transference numbers mean there is less concentration polarization and smaller concentration gradients across the electrolyte. Accordingly, batteries with inorganic SSEs have the potential to charge/discharge more rapidly and deliver higher power densities with significantly lower degradation than their liquid electrolyte

[z]E-mail: albertus@umd.edu

counterparts. Thus far, however, inorganic SSEs have struggled to live up to their potential due to interfacial and processing challenges. As a result, there is a continued effort to search for alternative electrolytes.

In our previous work we have developed a Cu^{2+}-doped cellulose-nanofiber (Cu-CNF) based electrolyte that has demonstrated great potential for high ion transport performance under high charging rates. As shown in Fig. 1, Cu-CNF consists of a random network of cellulose nanofibers that are doped with Cu^{2+} to promote Li^+ incorporation and transport within the fibers.[6] Cu-CNF has many favorable properties. First, it has low density, which is beneficial to cell specific energy. Cu-CNF has a density of about 1.1 g cm^{-3}, which compares favorably with sulfides/argyrodites[7] (~1.9 g cm^{-3}), and LLZO[8] (about 5.1 g cm^{-3}). Second, cellulose fibers are flexible and can produce a flexible separator. Plastic flow under compressive pressure from calendaring reduces void volume, which, thereby, favors dendrite suppression.[9] Third, Cu-CNF can be processed in a slurry form for use in cathodes, which is, comparatively, very challenging for typical particle-based ceramics because of the challenge of removing inter-particle voids and ensuring good interfacial contact at the commercially relevant stack pressure of <1 MPa.[10,11]

Despite these advantages, Cu-CNF is challenging to analyze and develop as an electrolyte because it is multi-component and has a morphologically hierarchical structure. As shown in Fig. 1, the Cu-CNF material is composed of fibers, within which are several species involved in ion transport. The Cu-CNF material has been immersed in a (non-aqueous) liquid electrolyte (e.g. 1 M LiTFSI in EC+DMC solvent) for ion exchange to provide for transport within and between the cellulose nanofibers. Following ion exchange, the material is dried by pressing, but some residual bound water due to the strong hydrogen bond with cellulose and some residual solvent still exist in the Cu-CNF. The present study examines two formulations of the Cu-CNF solid electrolytes, E-1 and E-2. The E-1 formulation consists of the Cu-CNF electrolyte with EC+DMC residual solvent, while the E-2 electrolyte consists of the Cu-CNF electrolyte with FEC+EMC residual solvent. Some of the Li^+ ions in the nanofibers are charge balanced by immobile carboxylate (COO^-) and alkoxide (RO^-) ions. The remaining Li^+ ions in the electrolyte are charge balanced by mobile anions from the LiTFSI salt. The system also has internal structuring from the fibers, and related anisotropy. The Cu-CNF fibers are biopolymers that may undergo re-ordering in the presence of salt concentration gradients. In total, the Cu-CNF electrolyte in this work has at least six major components: Li^+ cations, bis(trifluoromethanesulfonyl) imide (TFSI) anions, cellulose fibers with bound Cu^{2+}, two or three organic residual solvents (depending on formulation), and a small amount (a few wt%) of water. Based on previous inductively coupled plasma (ICP) measurements, the Li^+ concentration is ~1.1 M, very similar to the ~1.14 M in the MD simulations in this work.[6] Residual solvent molecules and water have been shown to be critical in enabling Li-ion transport in the cellulose fibers.[6]

The binary salt diffusion coefficient (referred to this in paper as $D_{\pm}$) is well defined for systems consisting of a binary salt dissolved in a solvent or solvent mixture.[12,13] The present Cu-CNF system also has, to our understanding, a single mobile cation (Li^+) and anion ($TFSI^-$), although with numerous local solvation environments involving both fixed charges from CNF and mobile solvent molecules. Hence, there are conceptual complexities with applying a simple "binary salt in solvent" model to the Cu-CNF electrolyte. The methods employed in the present paper, which are restricted diffusion, nuclear magnetic resonance (NMR) and molecular dynamics (MD), provide values for $D_{\pm}$, D_{Li^+}, and D_{TFSI^-}. It will be discussed if comparison can be made as these values from different methods may measure or compute transport properties under different driving forces or conditions. Further work is needed on how these methods can be formally and specifically applied to each of the components and/or transport modes in the Cu-CNF system.

In this study, we report our measurements on diffusion within the Cu-CNF electrolyte, with the inclusion of experimental measurements and MD simulations on ionic conductivity for context. We leave studies on the transference number, and the influence of electrolyte composition on salt diffusivity and ionic conduction, to future work. For both the E-1 and E-2 formulations, we use restricted diffusion to obtain values for $D_{\pm}$, while for both NMR and MD we obtain values for the ion diffusivities of Li^+ and $TFSI^-$.

Methods

In the present section, we describe our methods for the restricted diffusion (RD), molecular dynamics (MD), and nuclear magnetic resonance (NMR)methods. Table S1 in the SI summarizes the characteristics of each method.

Restricted diffusion.—The restricted diffusion (RD) technique was developed from the study of standing waves in electrolytes by Harned and French.[14] Specifically, a galvanostatic current pulse is applied to a sample for a sufficiently long duration that a steady-state concentration gradient is established (with a small magnitude, e.g., 10% variation between the concentration maximum and minimum

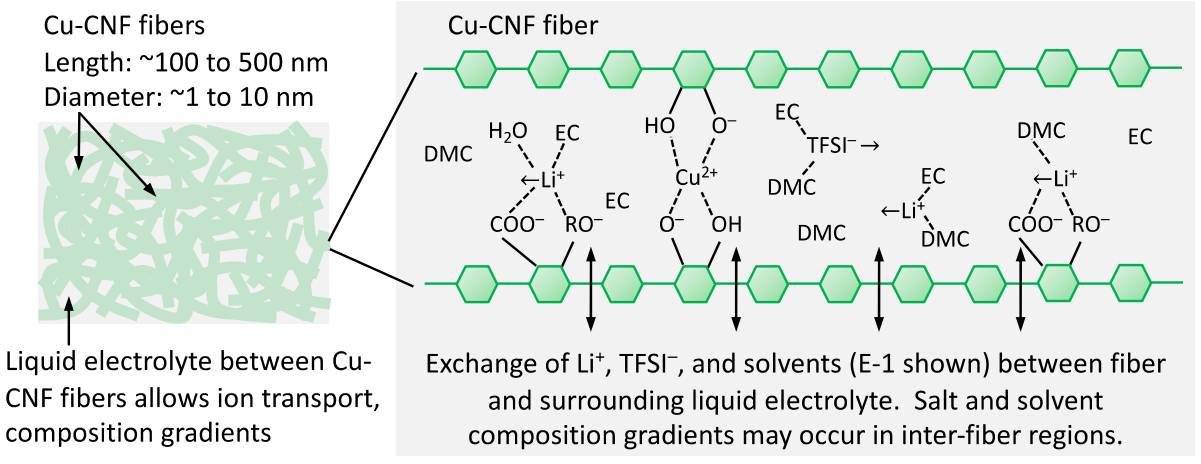

Composition: ~85 wt% fibers, ~15 wt% liquid electrolyte. E-1 (shown): LiTFSI in EC/DMC, E-2: LiTFSI in FEC/EMC

Figure 1. Schematic of Cu-CNF fiber-based electrolyte structure and composition used in our study. The cellulose nanofibers have Cu^{2+} coordinated to create space for Li^+ transport, as well as the $LiTFSI^-$ and some residual solvent molecules and H_2O for ion solvation. The Li^+:$TFSI^-$ ratio in the fibers is ~3:1, which indicates 2 of 3 Li^+ are charge balanced with –O– groups covalently bound in the cellulose fibers. The samples in this study are composed of ~85 wt% fibers and ~15 wt% liquid electrolyte, similar to a previous study.[6] Note: E-1 composition is shown above.

values, to limit the influence of convection during the relaxation, as well as avoid dendrite formation and electrode effects), and the restricted diffusion is monitored when the current is removed. During relaxation, the current is zero so there is no ohmic or kinetic polarization. A Fourier series model developed by Harned and French,[14] and later confirmed by Newman and Chapman[15] and Erhl et al.,[13] showed that the voltage relaxation profile obtained from RD experiments can be modeled by an exponential decay function that, for a given thickness and current amplitude, is only a function of $D_{\pm}$. Hence, RD experiments have been used to measure $D_{\pm}$ directly for both liquid and polymer electrolytes with the important advantage that $D_{\pm}$ can be obtained without the input of concentration values or the knowledge of any other transport property.[13–15]

Lithium-symmetric (8 mm or 6 mm diameter electrodes) coin cells consisting of 50 μm and 200 μm thick Cu-CNF electrolytes with E-1 and E-2 compositions were fabricated as described in previous work.[6] The coin cell hardware results in the presence of some applied pressure on the cell layers (i.e., a few bar). The cells were placed in a Tenney T2C-A-F4T environmental chamber to set the testing temperature. Isothermal restricted diffusion experiments were then conducted for select temperatures in the range −5 °C to +45 °C. The current protocol and sample relaxation data are shown in Fig. 2. An Arbin LBT 200084 galvanostat was used to apply a constant current to the coin cells. The current was then interrupted to allow the cell voltage to relax over time. After relaxation, a current of the same magnitude was then applied in the opposite direction for an identical time period, which was again followed by current interruption and a relaxation step. This cycle was run up to three times for each current applied to the cells. In addition, this three-cycle sequence was completed for several current densities to allow us to quantify the impact of both the direction and magnitude of the current density on the voltage relaxation results. The restricted diffusion data was then processed to obtain $D_{\pm}$ from the linear region of the voltage vs time relaxation profiles using the following equation:

$$D_{\pm} = \frac{L^2}{\pi^2} \cdot \underbrace{\frac{\mathrm{d}(\ln(|V - V_{offset}|))}{\mathrm{d}t}}_{slope} \quad [1]$$

where L is the electrolyte (Cu-CNF) thickness, t is time, and V is the measured voltage. V_{offset} is the absolute minimum voltage during a relaxation if the current density was positive, or the absolute maximum voltage if the current density was negative. As Ehrl et al.[13] show, the cell voltage (V) does not relax exactly to zero, therefore it is necessary to fit the relaxation curves with an offset voltage (V_{offset}). An example of V_{offset} is shown in Fig. 2b. A fitting window of 0.5 to 2 mV from V_{offset} was used.

Ionic conductivity measurements.—Ionic conductivity measurements were conducted in a coin cell configuration for E-1 and E-2 samples. Stainless steel blocking electrodes were used, and EIS spectra were collected using a 10 mV potential amplitude and a frequency range of 10 mHz to 200 kHz, from which the high-frequency resistance was extracted to obtain the ionic conductivity value. The thickness of each sample was 50 μm. Prior to measuring ionic conductivity, the cell was equilibrated for 30 min in an environmental chamber (Tenney T2C-A-F4T) to reach the set temperature.

Nuclear magnetic resonance spectroscopy.—Nuclear Magnetic Resonance is a powerful tool that provides quantitative and qualitative information at the molecular level, which helps in

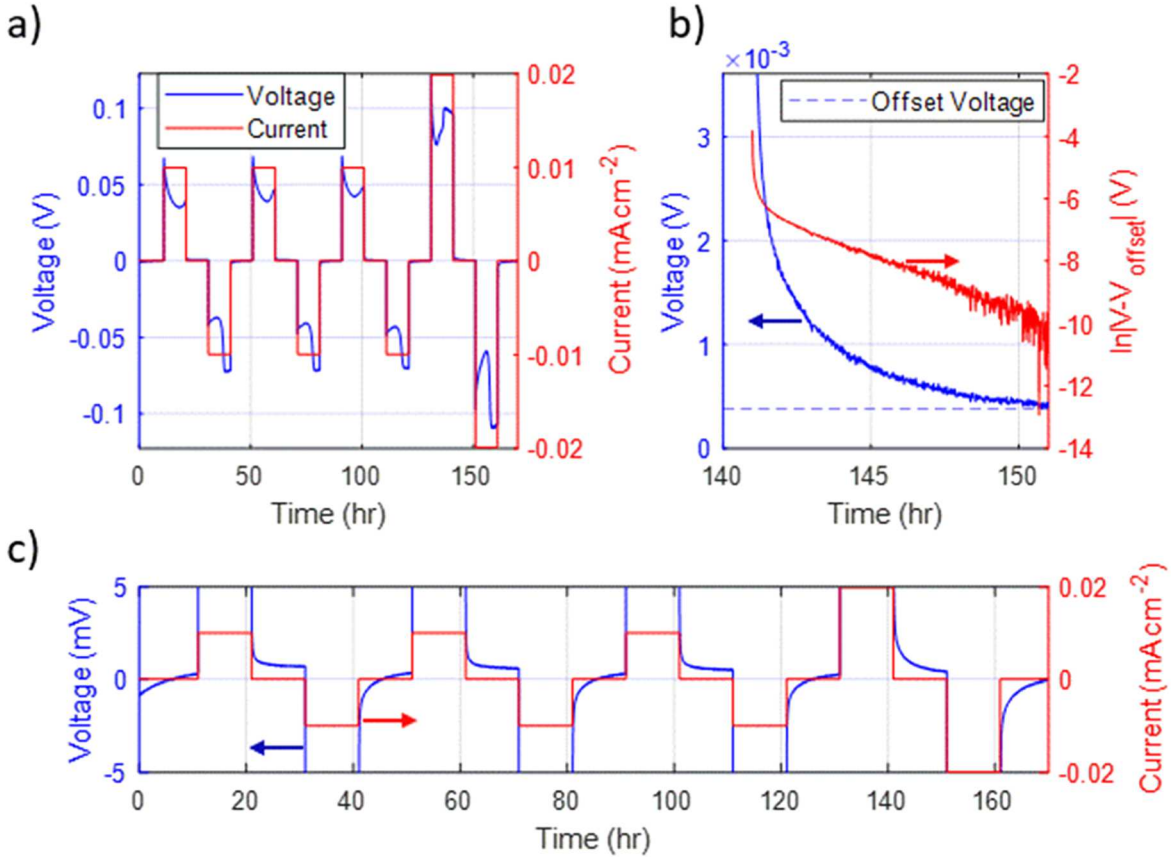

Figure 2. (a) Example of galvanostatic currents (red lines) applied to LilCu-CNFlLi symmetric cells and the voltage response (blue lines) (b) Example of a voltage relaxation curve, i.e., the voltage response when the current is switched off. The dashed line is the offset voltage which is the distance away from zero at the end of the relaxation period. (c) Close-up of the current steps and voltage relaxations for the same data shown in panel (a).

understanding the structure and dynamics of various battery materials. Both Li^+ and $TFSI^-$ concentrations were determined by integration of the NMR signals in the sample, using reference solutions of known ionic concentration. The pulsed field gradient (PFG) NMR technique has been used to measure the self-diffusion coefficients of Li^+ and $TFSI^-$; ion motion is due to the Brownian motion of representative NMR active nuclei such as ^7Li and ^{19}F that displace from their initial position during the measurement.

Diffusion NMR measurements were performed on a 300 MHz NMR spectrometer equipped with a DOTY Z-spec PFG NMR probe at 46 °C for the E-1 formulation and 25 °C for the E-2 formulation. The stimulated echo pulse sequence was used to collect the ^7Li or ^{19}F signal by varying the gradient strength up to 900 G cm^{-1}. The signal was accumulated for 1024 transients with 2 s recycling delay. The ion diffusivities(D_{Li^+} and D_{TFSI^-}) were calculated by using the Stejkal-Tanner equation[16]

$$I = I_0 \exp\left(-\gamma^2 g^2 \delta^2 D\left(\Delta - \tfrac{1}{3}\delta\right)\right) \quad [2]$$

where I and I_0 are the intensity with and without field gradient, γ is the gyromagnetic ratio, g and δ are the gradient strength and duration, and Δ is the diffusion time.

Molecular dynamics.—To clarify the diffusion mechanisms, classical Molecular Dynamics (MD) simulations with the COMPASS III force field[17] were performed following the protocols established in our previous work.[6] The unique amorphous Cu-CNF structures were obtained from crystalline followed by a soaking and drying process mimicking the fabrication process. As shown in the previous work, 8 parallel cellulose chains, each with 27 anhydroglucose units (AGUs) with periodic boundary conditions, were modeled. Tables S2 and S3 list the detailed compositions and number of atoms for E-1 and E-2. Based on the volume of the system, the Li+ concentration is ∼1.14 M.

The COMPASS III force field,[18] well-parameterized for organic and inorganic small molecules as well as polymer systems,[19,20] was adopted to account for both the bonded and non-bonded interactions. The atomic charges of Li^+ and anions (COO^-, RO^-, and $TFSI^-$) are scaled by 0.7 to effectively introduce electronic polarizations, and all other details of the force field parameters can be found in our previous publication.[6] Density functional theory (DFT) calculations were conducted to calculate the binding energies between Li+ and TFSI- and other species using the M06–2X[21] functional, the 6–31+G (d,p) basis set and the D3 dispersion correction[22] as implemented in Gaussian 09 code (version D.01).[23] See figure S5(d) for more information.

All molecular dynamics (MD) simulations of the E-1 and E-2 formulations of the Cu-CNF electrolytes were conducted using the Forcite module in Materials Studio[24] by starting with a 2.0 ns simulation under the ensemble with constant number, pressure, and temperature (NPT) to obtain a relaxed simulation box. Then a 2.0 ns simulation under the constant number, volume, and temperature (NVT) ensemble was conducted for equilibration followed by a 10.0 ns NVT simulation as production run to investigate transport properties. The ion diffusivities and activation energies are calculated following the method described in the literature.[25] Through MD simulations, one can calculate the self-diffusion coefficients of both cations and anions by a linear fitting of the mean square displacements as functions of time.[25,26] The MD simulations were conducted at several high temperatures (550 K, 600 K, 650 K, 700 K, and 800 K) to accelerate dynamics, and then an Arrhenius plot constructed to extrapolate ion diffusivities to 45 °C, a temperature at both restricted diffusion and NMR measurements were carried out.

Results and Discussion

The present section presents our results on the E-1 and E-2 compositions from RD experiments, NMR experiments, and MD modeling. For RD, we completed >100 individual relaxations among the E-1 and E-2 samples at a range of temperatures, applied currents, cycle counts, and positive vs negative currents. For NMR we carried out two experiments, one on E-1 (at 46 °C) and one on E-2 (at 25 °C). For the MD simulations, we analyzed four systems, two composition variants based on E-1 and two composition variants based on E-2.

Restricted diffusion.—Figure 2a shows an example of the galvanostatic currents applied to the Li|Cu-CNF|Li symmetric cells. The voltage response when the current is on (e.g., showing both increases and decreases in magnitude) likely reflects the microstructural evolution of the lithium electrode interface. After the current is switched off ($i = 0$) the voltage relaxes, Fig. 2b, as the concentration overpotential in the cell relaxes.

The relaxation curves are not perfectly linear over the entire voltage relaxation. Therefore, it was necessary to choose a voltage-time window in which to carry out a linear fit of the voltage relaxation. Figure 3 shows the voltage relaxation profiles following a 0.1 mA cm^{-2} galvanostatic current at 25 °C and 45 °C for the E-1 Cu-CNF formulation. The plots show that there is a linear region that is not significantly affected by noise. Within this fitting window (0.5 to 2 mV above the cutoff voltage), 70 out of 104 of the lines (slopes) used to calculate the $D_\pm$ values have a correlation coefficient (R^2) greater than or equal to 0.95, and 100 of 104 have an R^2 greater than or equal to 0.9. This confirms that the profiles of the curves were sufficiently linear within the 0.5 to 2 mV voltage relaxation window. Additional results and variations on our restricted diffusion analysis are contained in the Supporting Information in Figs. S1 to S4.

The plots in Fig. 3 also show a difference in the slope between the first cycle and the third cycle (for brevity, the second cycle is not shown) and a much larger slope change when the direction of the pulse is reversed. The effects of the cycle number on $D_\pm$ are small enough that they might be attributable to minor physical changes in the cell over cycling and time. However, the differences in the results for $i > 0$ and $i < 0$ are likely due to the asymmetric variations in the solid electrolyte interphase (SEI) as also affected by temperature, current density magnitude, and sample composition; furthering studying and quantifying these asymmetries is an important area for future work. Hence, the $D_\pm$ values obtained from each cycle (i.e., pairs of $i > 0$ and $i < 0$) were averaged.

Figure 4 shows examples of how the $D_\pm$ values change for each cycle for both positive and negative applied current densities, and several current density magnitudes, for the E-1 formulation at 45 °C; the variance here is comparable to previous publications using the RD method, and previous publications also observed differences in $D_\pm$ for $i > 0$ vs $i < 0$.[13,27] Further work is needed to identify the mechanism(s) causing variance in $D_\pm$ results among cycle number and current direction. Note that Fig. S4 includes further quantitative information on the relation between $D_\pm$ and the current density magnitude.

Figure 5 summarizes the $D_\pm$ values obtained from all the RD experiments as a function of temperature. The data points represent the average values of $D_\pm$ for a given temperature and formulation. The variance between the upper and lower standard deviations in the $D_\pm$ data is about a factor of 3. We note that Hou and Monroe[12] and Ehrl et al.[13] show similar variance in experimental measurements of $D_\pm$. Statistical analysis of our data suggests that approximately 80% of the variance observed in Fig. 5 arises from sample-to-sample variance, while the rest comes from the effects of the cycling conditions (e.g., the current density magnitude as shown in Fig. S4). Moreover, the complexity of the Cu-CNF system means that there are multiple contributors to the concentration overpotential in the electrolyte, which may increase the sample-to-sample variance.

Ionic conductivity.—While not a focus of the present paper, as an additional point of reference in Fig. 6 we present results of ionic conductivity measurements for both E-1 and E-2 Cu-CNF formulations. Ionic conductivity measurements were made using stainless

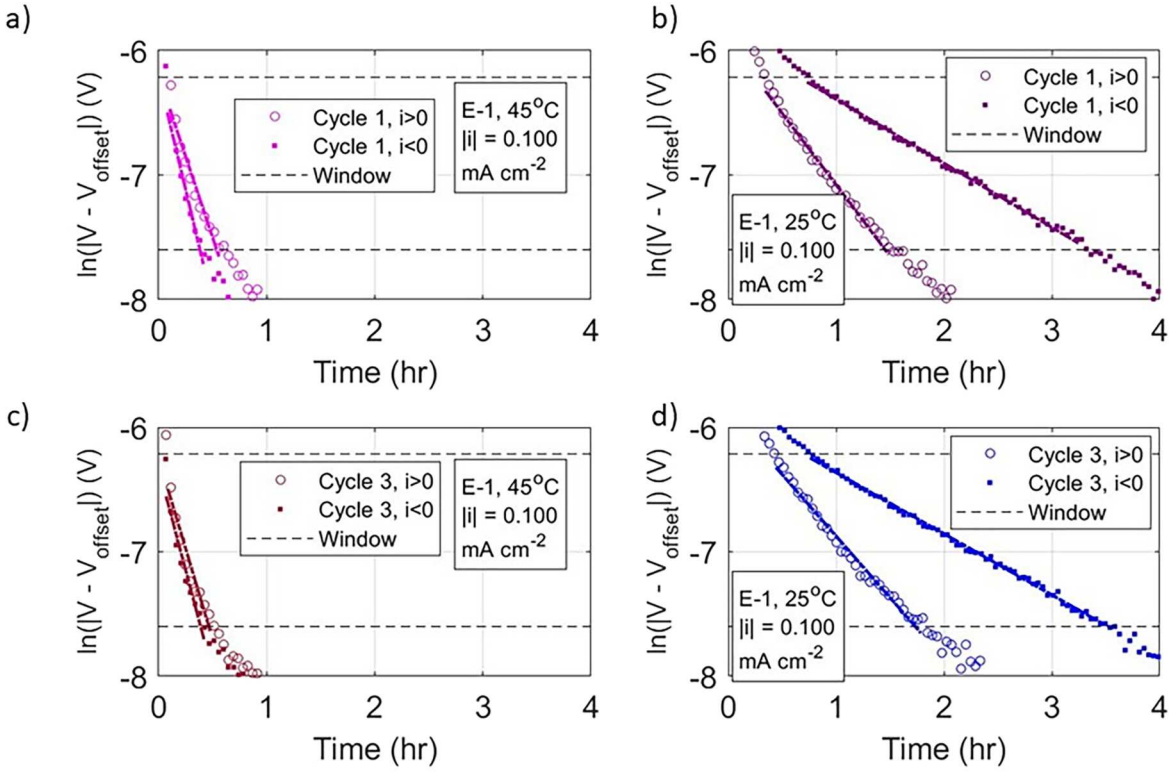

Figure 3. Relaxation data for the 200 μm-thick E-1 formulation of the Cu-CNF electrolyte showing the fitting window (dashed lines) and cycle numbers for 25 °C and 45 °C: (a) 45 °C, cycle 1; (b) 25 °C, cycle 1; (c) 45 °C, cycle 3; and (d) 25 °C, cycle 3. The lines of best fit are also included in the panels above.

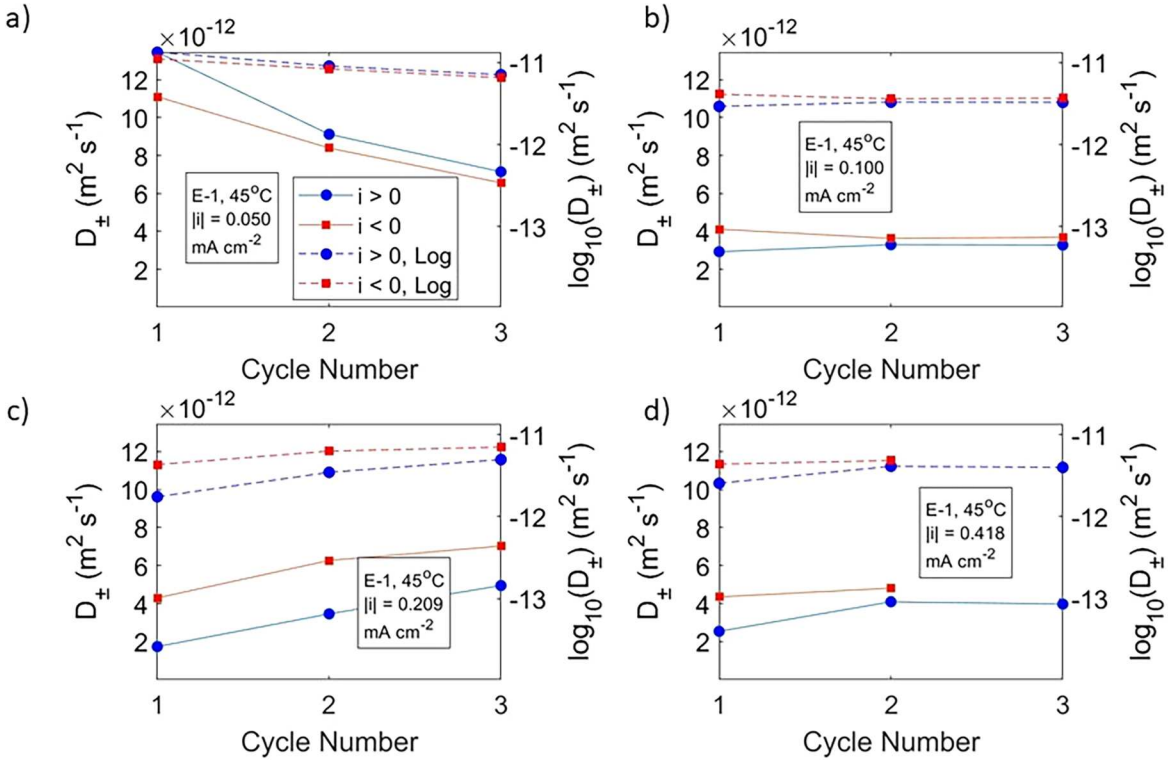

Figure 4. Relaxation data showing the change in the $D_{\pm}$ values as a function of the cycle number for a 200 μm-thick Cu-CNF sample with the E-1 formulation at 45 °C for applied currents of (a) 0.050 mA cm^{-2}, (b) 0.100 mA cm^{-2}, (c) 0.209 mA cm^{-2}, and (d) 0.418 mA cm^{-2}. The dashed lines correspond to the logarithmic *y*-axis (right side) and the solid lines correspond to the linear *y*-axis (left side). *i* is the applied current, and the blue circles represent $i > 0$ and the red squares represent $i < 0$.

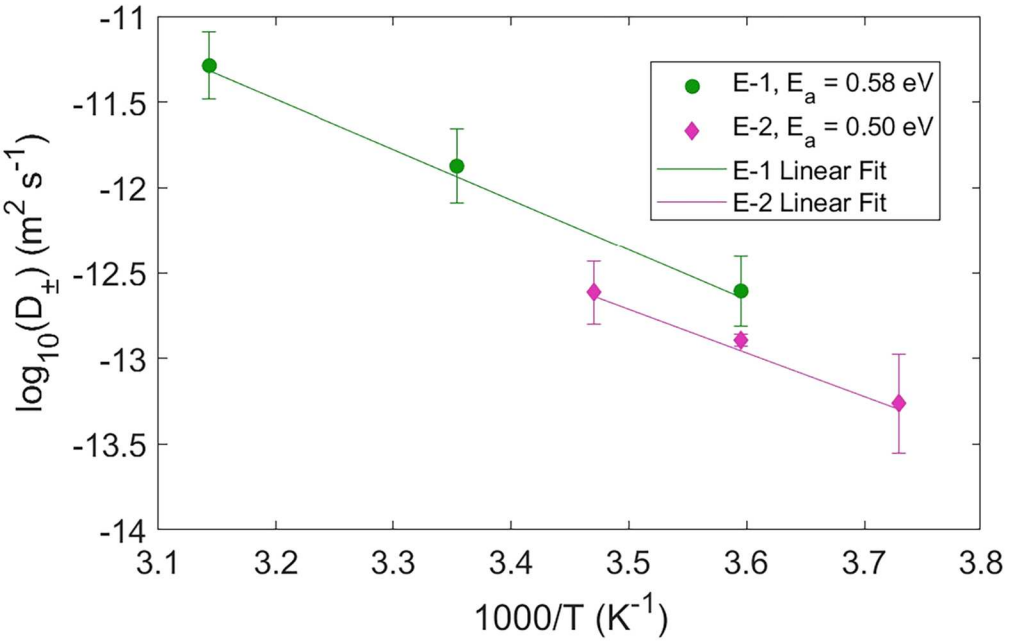

Figure 5. Temperature dependence of $D_{\pm}$ as measured by restricted diffusion for E-1 and E-2 formulations of Cu-CNF. For each temperature and formulation, the $D_{\pm}$ values obtained from fitting the linear regions of relaxations from each trial to Eq. 1 were averaged and used to calculate standard deviations. Uncertainty bars indicate one standard deviation. The results are based on >100 voltage relaxations.

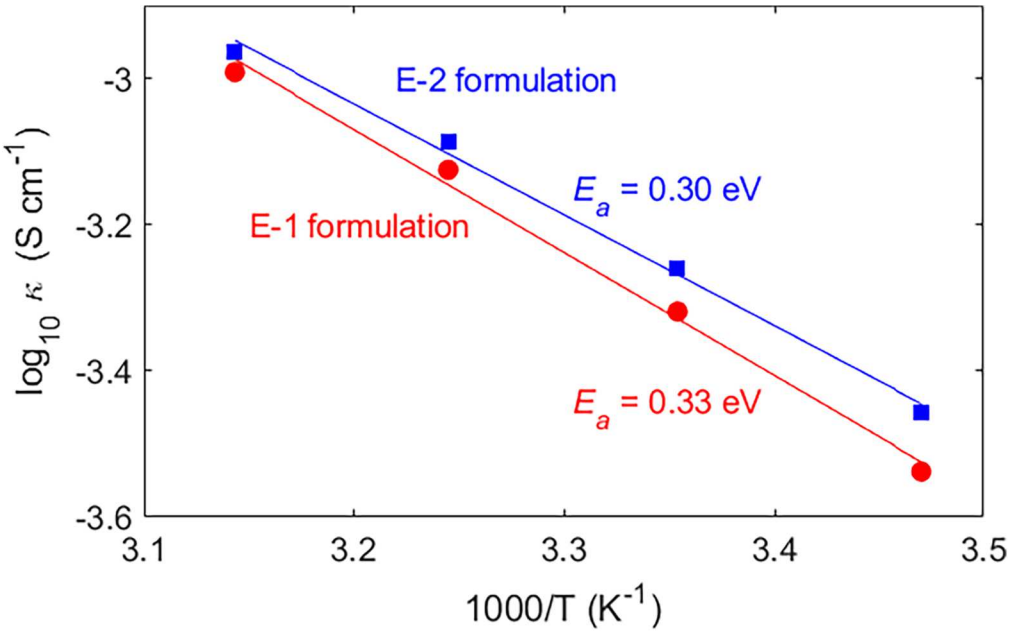

Figure 6. Temperature dependence of ionic conductivity, κ, for E-1 and E-2 formulations of Cu-CNF electrolytes. Activation energies, E_a, are also provided.

steel blocking electrodes for both E-1 and E-2 formulations of Cu-CNF in the temperature range 15 °C to 45 °C. See the SI and figure S5 for more information. Figure 6 shows that the E-2 Cu-CNF formulation has a slightly lower activation energy and higher conductivity than the E-1 formulation. The through-plane ionic conductivities at 25 °C for these Cu-CNF samples are about 0.5 × 10^{-3} S cm^{-1}, and the activation energies are about 0.3 eV. For reference, a commercial liquid Li-ion electrolytes has a pure-phase ionic conductivity of ∼10 × 10^{-3} S cm^{-1} at 25 °C.[28] However, its effective ionic conductivity in a porous separator with a porosity of 0.4 is about 8x lower than the pure liquid phase,[29] so the effective ionic conductivity of the Cu-CNF material is within ∼2x of a liquid electrolyte in a porous separator.

Nuclear magnetic resonance (NMR).—The Cu-CNF samples were also measured by PFG-NMR; results are shown in Fig. 7. Results for E-1 (Figs. 7a and 7b), at 46 °C, show single narrow ^{7}Li and ^{19}F peaks were observed in the corresponding NMR spectra and indicate that both ions are mobile. These spectra also highlight the absence of multiple Li^{+} or $TFSI^{-}$ environments. Moreover, the intensity vs gradient plots of both D_{Li+} and D_{TFSI-} were obtained by measuring an average diffusion coefficient for ions moving within the fibers and between the fibers. The ions in these two environments undergo rapid exchange compared to the timescale of the NMR measurement. The concentrations of Li^{+} and $TFSI^{-}$ were estimated by collecting 1D NMR spectra and referencing to the standard. The estimated Li^{+}:$TFSI^{-}$ ratio is 1:0.3. Similar steps were applied for

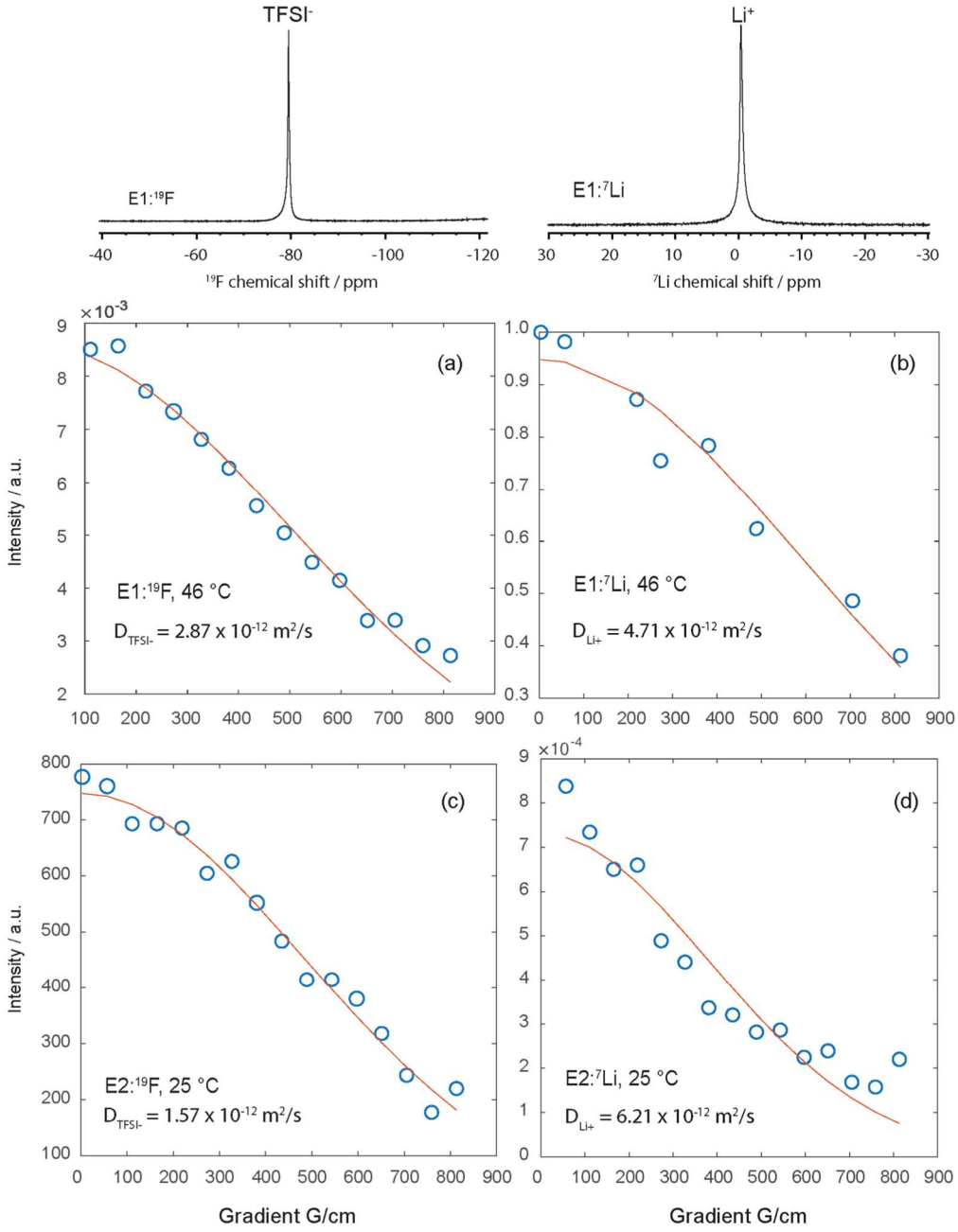

Figure 7. PFG-NMR results. The top two panels show ^{19}F spectra and ^{7}Li spectra for the E-1 Cu-CNF electrolyte. Diffusion plots for the E-1 (a) ^{19}F and (b) ^{7}Li and E-2 (c) ^{19}F and (d) ^{7}Li formulations are also shown. The E-1 experiments were done at 46 °C and the E-2 experiments at 25 °C.

Table I. MD-simulated systems: E-1 electrolyte with LiTFSI-EC-DMC and E-2 electrolyte with LiTFSI-FEC-EMC. See the table of abbreviations for more information.

E-1: LiTFSI-EC-DMC			E-2: LiTFSI-FEC-EMC		
#	label	Li:TFSI	#	label	Li:TFSI
1	Cu-18AGU-**3Li-TFSI**-2EC-2DMC-2H_2O	3:1	3	Cu-18AGU-**3Li-TFSI**-2FEC-2EMC-2H_2O	3:1
2	Cu-18AGU-**3Li-2TFSI**-2EC-2DMC-2H_2O	3:2	4	Cu-18AGU-**3Li-2TFSI**-2FEC-2EMC-2H_2O	3:2

sample E-2, with results shown in Figs. 7c and 7d. Quantitative analysis revealed in this case a Li^+:$TFSI^-$ ratio of 1:0.87. Figures 5 and 7 show that the values for D_{Li^+} and D_{TFSI^-} from NMR measurements are similar to the values of $D_{\pm}$ from RD at equivalent temperatures. See the SI and Fig. S6 for more information.

***Molecular dynamics.*—**Table I shows the list of the E-1 and E-2 electrolytes along with their chemical compositions for MD simulations. The model for the E-1 electrolyte was first built with Li^+/$TFSI^-$ ratio of 3:1, inspired by the experimental Li^+/$TFSI^-$ ratio of 1:0.3 as measured with NMR Details of settings for the MD

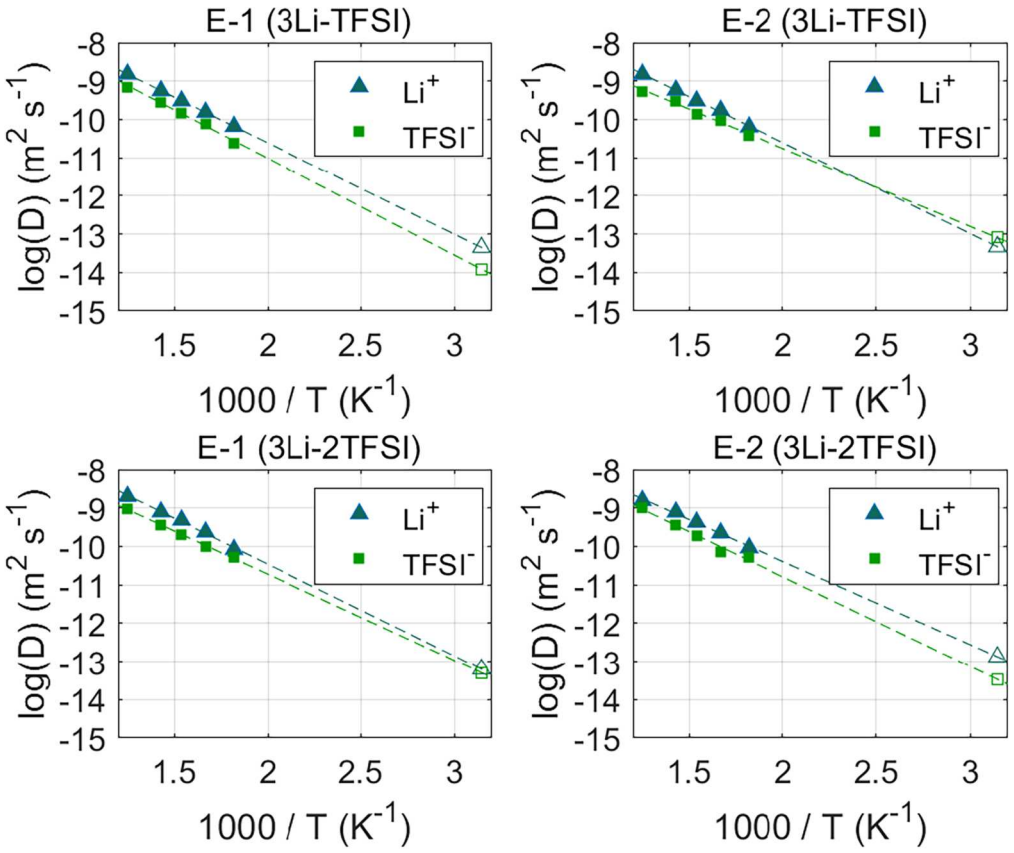

Figure 8. Arrhenius plots of Li^+ and $TFSI^-$ diffusivity for E-1 and E-2 electrolytes with different Li-TFSI ratios (3Li-TFSI and 3Li-2TFSI).

Table II. Activation energies of Li^+ and $TFSI^-$ diffusivities for E-1 and E-2 electrolytes with different Li^+-$TFSI^-$ ratios (3:1 and 3:2) obtained from MD simulations.

Electrolyte	Li^+:$TFSI^-$	E_a (Li^+) (eV)	E_a ($TFSI^-$) (eV)
E-1	3:1	0.21	0.22
	3:2	0.21	0.19
E-2	3:1	0.21	0.18
	3:2	0.19	0.20

model are given in table S2 (for E-1 electrolyte) and table S3 (for E-2 electrolyte) of the SI. For the E-2 electrolyte, NMR found a $Li^+/TFSI^-$ ratio of about 1:0.87. In the MD simulations, we have considered the $Li^+/TFSI^-$ ratios of 3:1 and 3:2 for both E-1 and E-2 electrolytes. The ratios of bound water and solvent molecules in the E-1 electrolyte were also taken from NMR measurements for the E-1 electrolyte, and these ratios are kept in the simulations of the E-2 electrolyte.

Similar to hybrid ion transport mechanisms observed in Cu-CNT with only bound water,[6] Li^+ ions hop with assistance from the small molecules (H_2O, EC, and DMC). In contrast, the transport of $TFSI^-$ follows a vehicular mechanism (randomly moving without being dragged by the residual molecules), as verified by the absence of highly structured coordination environments for $TFSI^-$ (Fig. S7). This is consistent with the fact that the pair-wise interactions between $TFSI^-$ and the other moieties (AGU, EC, DMC, and H_2O) are all significantly smaller than the interactions between Li^+ and these moieties, as shown by the DFT-calculated binding energies (Fig. S7).

Figure 8 shows the diffusion coefficients of Li^+ and $TFSI^-$ at different temperatures for E-1 and E-2 electrolytes with different $Li^+/TFSI^-$ ratios (3:1 and 3:2). MD simulations were performed at higher temperatures (550–800 K) to accelerate dynamics and potentially include some chain mobility contributions to the ion conductivity that are beyond the MD simulation time at room temperature. See Figs S8 and S9 for the mean-square displacement (MSD) plots. Then diffusion coefficients were extrapolated to 45 °C through fitting following an Arrhenius plot for comparison with RD and NMR measurements; see Tables S4 and S5. At all temperatures, Li^+ moves faster than $TFSI^-$. The activation energies, in Table II, are calculated to be around 0.20 eV for both Li^+ and $TFSI^-$. Figure S10 shows the corresponding total ionic conductivities based on the diffusivity data of Fig. 8, following the Nernst−Einstein equation. Fully correlated ionic transport following Green–Kubo relation will be presented in the future, since the current NMR measurements also ignored ion correlations. As shown in Tables S4 and S5, the existence of the residual solvent and water molecules has a positive impact on the transport of Li^+, and its impact on the transport of $TFSI^-$ is even stronger. In the presence of EC, DMC, and H_2O, the diffusion coefficient of $TFSI^-$ is slightly smaller than that of Li^+, but they are in the same order of magnitude, as revealed by both MD simulations for E-1 electrolyte ($Li^+/TFSI^-$ ratio is 3:1 in this case) and NMR measurement. However, in the absence of EC, DMC, and H_2O, the diffusion coefficient of $TFSI^-$ is two orders of magnitude smaller than that of Li^+ (Table S5). As a result, the activation energies become significantly higher for both Li^+ and $TFSI^-$ in the absence of the solvent and water molecules. This is likely due to the larger size of the $TFSI^-$ and the inter-chain space created by Cu^{2+}-coordination that is ideal for Li^+ but not $TFSI^-$ transport.

To conclude, we have established atomistic models for both E-1 and E-2 electrolytes with different $Li^+/TFSI^-$ ratios and performed MD simulations to investigate the structural and transport properties, by making systematic comparisons between the E-1 and E-2 electrolytes, as well as comparisons between MD simulations and experiments. We have revealed the transport mechanism of Li^+ ions to be hopping with assistance by small molecules, and the transport mechanism of $TFSI^-$ to be a vehicular mechanism.

Comparing restricted diffusion, ionic conductivity, NMR, and molecular dynamics results.—Comparing Figs. 5, 7, and 8, we see that while the RD and NMR methods give similar values for salt diffusivity and ion diffusivities (about 5×10^{-12} m^2 s^{-1} at 45 °C), MD results indicate a value about 100x lower. In addition, while there are only two NMR measurements, so an activation energy cannot be obtained from that method, RD and MD results show a significant difference in activation energy for salt diffusivity (about 0.55 eV for RD, and 0.20 eV for MD). The activation energy from MD (0.20 eV) is closer to the experimental activation energy for ionic conductivity (0.3 eV). In MD simulations, the two properties have the same activation energy. We identify several possible explanations for differences in diffusivities and their activation energies among the three methods. First, those differences may come from the fact that the MD only treats intra-fiber transport, while the RD and NMR include all transport pathways (including intra- and inter-fiber transport). The MD simulations also distributed all the residual molecules within the fiber, while in experiments, more residual molecules may fill the inter-chain space. Second, differences may arise from the construction of the MD, RD, and NMR approaches; in particular, MD is built around following ion motion in random walks at an equilibrium condition, while RD follows the relaxation to equilibrium of a system whose composition has been perturbed by the passage of current. NMR is also done around an equilibrium condition rather than following relaxation from a long-length-scale (10 s of microns in the case of RD) perturbation in composition. Third, differences in ion diffusivities and their activation energies may result from relaxation processes in the cellulose chain that occur over minutes to hours in the RD tests that are not present in the NMR and MD experiments that measure ion diffusivities over much shorter time increments. As discussed above, the use of an elevated temperature for the MD experiments and the use of the Arrenhius equation to estimate ion diffusivities at 45 °C, may also affect how MD results reflect cellulose chain relaxation processes. Fourth, differences among the methods may also result from the presence of complex speciation processes in this Cu-CNF system, including ion-ion association. For example, previous detailed experimental work on transport properties in three liquid electrolytes found that for three electrolyte compositions there could be significant (∼2x) differences in ionic conductivity while the salt diffusivities among the three compositions were nearly identical.[28,30] As a result of these four factors, and potentially others, additional work will be needed to strengthen the ability to interpret and compare results from each method. A promising experimental approach to assist this effort would be to prepare a set of samples with systematically varying fractions of key components (e.g., salt, solvents, water) and apply each method to obtain transport properties.

A second major area for future work is to study the different ratios between the ionic conductivity of a typical commercial liquid electrolyte vs our Cu-CNF samples (the liquid electrolyte is about 20x more conductive at 25 °C) and the salt diffusivity of a typical commercial liquid electrolyte vs our Cu-CNF samples (the $D_{\pm}$ for the liquid electrolyte is about 300x higher at 25 °C). We also found a value of E_a for the Cu-CNF $D_{\pm}$ (0.50 to 0.58 eV) that was significantly higher than the E_a for ionic conductivity of Cu-CNF (∼0.3 eV), as well as E_a for ionic conductivity and salt diffusivity of a typical commercial liquid electrolyte (both ∼0.25 to 0.3 eV).[28] The different ratios among salt diffusivity, ionic conductivity, and their activations energies, may arise from ion-ion speciation effects particularly strong in this system, which have previously been used to explain, for a liquid electrolyte, changes in ionic conductivity but not salt diffusivity among different electrolyte compositions.[28,30] (Also mentioned in the previous paragraph). Another possible reason is that the measurements for $D_{\pm}$ average over a longer time span than the ionic conductivity measurements, such that some long time-scale processes are present in the RD measurements but not the ionic conductivity measurements. Careful experimental studies on how the multi-component and structured nature of the Cu-CNF electrolyte affects speciation and both ionic conductivity and salt diffusivity are needed.

Conclusions

To investigate transport in Cu-CNF electrolytes, restricted diffusion (RD) experiments were conducted on two formulations of Cu-CNF samples (E-1 and E-2) to obtain salt diffusivity, $D_{\pm}$, as a function of temperature. In addition, NMR and MD were used to obtain ion diffusivities, D_{Li^+} and D_{TFSI^-}. The approximate value of $D_{\pm}$ obtained from RD for Cu-CNF is 5×10^{-12} m^2 s^{-1} at 45 °C, and the ion diffusivities obtained from NMR have a similar value. The MD simulations found that Cu-CNF fibers have about a 100x lower value for ion diffusivities at 45 °C and an activation energy for Li^+ transport in a fiber of ∼0.21 eV. RD experiment on Cu-CNF samples yielded a much higher activation energy of 0.50 to 0.58 eV, and direct measurements of ionic conductivity on similar samples found an E_a value of ∼0.30 eV. We hypothesize that the development and relaxation of salt concentration gradients within and between fibers may account for differences in salt diffusivity and ion diffusivities for RD vs MD and NMR measurements, as well as differences in E_a values. Cellulose fiber chain rearrangement that occurs over the longer time scales of RD measurements may be an important contributor to the differences in transport properties assessed through these methods. We also identified how speciation effects, in particular ion-ion associations, could influence both the measured transport properties and differences in results among methods. The fundamental differences in how the methods assess transport—in particular, whether it from relaxation from a perturbed composition over 10 s of microns (RD) or at an equilibrium condition (NMR and MD)—may also account for some of the differences.

To further examine transport in Cu-CNF it would be helpful to conduct RD, MD, and NMR experiments to obtain the dependence of both $D_{\pm}$ and ionic conductivity on salt concentration and other controllable compositional variables. This would aid in furthering our understanding of different modes of transport within multi-component and structured electrolytes.

ORCID

Keith Duncan https://orcid.org/0000-0002-7190-3675
Qisheng Wu https://orcid.org/0000-0001-9123-1864
Mounesha Garaga https://orcid.org/0000-0003-0174-7934
Michael McKee https://orcid.org/0009-0004-5388-7458
Lin Xu https://orcid.org/0000-0002-3863-0214
Xueying Zheng https://orcid.org/0009-0002-8765-3348
Aysha Siddika Asha https://orcid.org/0000-0002-3710-1599
Yue Qi https://orcid.org/0000-0001-5331-1193
Steven Greenbaum https://orcid.org/0000-0001-5497-5274
Liangbing Hu https://orcid.org/0000-0002-9456-9315
Paul Albertus https://orcid.org/0000-0003-0072-0529

References

1. L. Usai, J. J. Lamb, E. Hertwich, O. S. Burheim, and A. H. Strømman, "Analysis of the Li-ion battery industry in light of the global transition to electric passenger light duty vehicles until 2050." *Environ. Res. Infrastruct. Sustain.*, **2**, 011002 (2022), 10.1088/2634–4505/ac49a0.
2. P. Albertus, S. Babinec, S. Litzelman, and A. Newman, "Status and challenges in enabling the lithium metal electrode for high-energy and low-cost rechargeable batteries." *Nat. Energy*, **3**, 16 (2018).
3. S. Link, L. Schneider, A. Stephan, L. Weymann, and P. Plötz, "Feasibility of meeting future battery demand via domestic cell production in Europe." *Nat. Energy*, 1 (2025).
4. M. Armand et al., "Lithium-ion batteries—current state of the art and anticipated developments." *J. Power Sources*, **479**, 228708 (2020).
5. J. Xu, X. Cai, S. Cai, Y. Shao, C. Hu, S. Lu, and S. Ding, "High-energy lithium-ion batteries: Recent progress and a promising future in applications." *ENERGY Environ. Mater.*, **6**, e12450 (2023).
6. C. Yang et al., "Copper-coordinated cellulose ion conductors for solid-state batteries." *Nature*, **598**, 590 (2021).
7. C. A. Heck, T. Scharmann, M. Osenberg, A. Diener, I. Manke, P. Michalowski, and A. Kwade, "Opportunities and challenges of calendering sulfide-based separators for solid-state batteries." *Batter. Supercaps*, **7**, e202300487 (2024).

8. W. Feng, Y. Zhao, and Y. Xia, "Solid interfaces for the garnet electrolytes." *Adv. Mater.*, **36**, 2306111 (2024).
9. D. Cao, X. Sun, Q. Li, A. Natan, P. Xiang, and H. Zhu, "Lithium dendrite in all-solid-state batteries: growth mechanisms, suppression strategies, and characterizations." *Matter*, **3**, 57 (2020).
10. H. Al-Salih, M. S. E. Houache, E. A. Baranova, and Y. Abu-Lebdeh, "Composite cathodes for solid-state lithium batteries: 'Catholytes' the underrated giants." *Adv. Energy Sustain. Res.*, **3**, 2200032 (2022).
11. C. Park, S. Lee, K. Kim, M. Kim, S. Choi, and D. Shin, "Electrochemical properties of composite cathode using bimodal sized electrolyte for all-solid-state batteries." *J. Electrochem. Soc.*, **166**, A5318 (2019).
12. T. Hou and C. W. Monroe, "Composition-dependent thermodynamic and mass-transport characterization of lithium hexafluorophosphate in propylene carbonate." *Electrochim. Acta*, **332**, 135085 (2020).
13. A. Ehrl, J. Landesfeind, W. A. Wall, and H. A. Gasteiger, "Determination of transport parameters in liquid binary lithium ion battery electrolytes: I. Diffusion coefficient." *J. Electrochem. Soc.*, **164**, A826 (2017).
14. H. S. Harned and D. M. French, "A conductance method for the determination of the diffusion coefficients of electrolytes." *Ann. N. Y. Acad. Sci.*, **46**, 267 (1945).
15. J. Newman and T. W. Chapman, "Restricted diffusion in binary solutions." *AIChE J.*, **19**, 343 (1973).
16. E. O. Stejskal and J. E. Tanner, "Spin diffusion measurements: spin echoes in the presence of a time-dependent field gradient." *J. Chem. Phys.*, **42**, 288 (1965).
17. R. L. C. Akkermans, N. A. Spenley, and S. H. Robertson, "COMPASS III: Automated fitting workflows and extension to ionic liquids." *Mol. Simul.*, **47**, 540 (2021).
18. H. Sun, Z. Jin, C. Yang, R. L. C. Akkermans, S. H. Robertson, N. A. Spenley, S. Miller, and S. M. Todd, "COMPASS II: Extended coverage for polymer and drug-like molecule databases." *J. Mol. Model.*, **22**, 47 (2016).
19. T. Ogoshi et al., "Molecular weight fractionation by confinement of polymer in one-dimensional pillar[5]arene channels." *Nat. Commun.*, **10**, 479 (2019).
20. L. Shi, X. Fu, Y. Li, S. Wu, S. Meng, and J. Wang, "Molecular dynamic simulations and experiments study on the mechanical properties of HTPE/PEG interpenetrating polymer network (IPN) binders." *Nanomaterials*, **13**, 268 (2023).
21. Y. Zhao and D. G. Truhlar, "The M06 suite of density functionals for main group thermochemistry, thermochemical kinetics, noncovalent interactions, excited states, and transition elements: two new functionals and systematic testing of four M06-class functionals and 12 other function." *Theor. Chem. Acc.*, **120**, 215 (2008).
22. S. Grimme, S. Ehrlich, and L. Goerigk, "Effect of the damping function in dispersion corrected density functional theory." *J. Comput. Chem.*, **32**, 1456 (2011).
23. M. J. Frisch et al., *09, Revision D.01*. (Gaussian, Inc, Wallingford CT) (2016).
24. Dassault Systèmes BIOVIA, *Materials Studio* (Dassault Systèmes, San Diego) (2020).
25. X. He, Y. Zhu, A. Epstein, and Y. Mo, "Statistical variances of diffusional properties from Ab Initio molecular dynamics simulations." *NPJ Comput. Mater.*, **4**, 18 (2018).
26. L. Bassman Oftelie et al., "Active learning for accelerated design of layered materials." *NPJ Comput. Mater.*, **4**, 1 (2018).
27. S. A. Mullin, G. M. Stone, A. Panday, and N. P. Balsara, "Salt diffusion coefficients in block copolymer electrolytes." *J. Electrochem. Soc.*, **158**, A619 (2011).
28. J. Landesfeind and H. A. Gasteiger, "Temperature and concentration dependence of the ionic transport properties of lithium-ion battery electrolytes." *J. Electrochem. Soc.*, **166**, A3079 (2019).
29. I. V. Thorat, D. E. Stephenson, N. A. Zacharias, K. Zaghib, J. N. Harb, and D. R. Wheeler, "Quantifying tortuosity in porous Li-ion battery materials." *J. Power Sources*, **188**, 592 (2009).
30. Z. Feng, K. Higa, K. S. Han, and V. Srinivasan, "Evaluating transport properties and ionic dissociation of LiPF6 in concentrated electrolyte." *J. Electrochem. Soc.*, **164**, A2434 (2017).